Absolute dielectronic recombination cross sections of hydrogenlike helium

D. R. DeWitt, R. Schuch, T. Quinteros, H. Gao, and W. Zong
Department of Atomic Physics, Stockholm University, S-104 05 Stockholm, Sweden*

H. Danared
Manne Siegbahn Laboratory, Stockholm University, S-104 05 Stockholm, Sweden

M. Pajek
Institute of Physics, Pedagogical University, 25-509 Kielce, Poland

N. R. Badnell
Department of Physics and Applied Physics, University of Strathclyde, Glasgow G40NG, Great Britain
(Received 18 November 1993)

We have measured the $\Delta N=1$ dielectronic recombination cross sections of hydrogenlike helium. Recombination rates were investigated as He^+ ions interacted with free electrons in the electron-cooler section of an ion storage ring. The ion beam was cooled prior to recombination, resulting in enhanced energy resolution. Fits to the $2l2l'$ resonances yielded transverse and longitudinal temperatures of $kT_\perp=0.15$ eV and $kT_\parallel=0.8\times10^{-4}$ eV, respectively. The resulting peak widths are approximately 0.3-eV full width at half maximum. The measured integrated cross sections are in qualitative agreement with calculated resonance strengths.

PACS number(s): 34.80.Kw

I. INTRODUCTION

Interest in dielectronic recombination [1,2] has intensified in recent years with the arrival of several new experimental techniques. Dielectronic recombination (DR) is a resonant process which plays an important role in plasma dynamics [3,4], and is also a subject of interest in studies of atomic structure. Among the recent experimental techniques, the observation of x rays [5,6] and extracted ions [7,8] from electron-beam ion traps, and recombination products from ion storage rings [9,10], have received a great deal of attention. Storage rings equipped with an electron cooler provide high-quality interaction conditions, high efficiency, and high-energy resolution. We used the cooler storage ring CRYRING in Stockholm to measure dielectronic recombination cross sections of He^+ ions. The process examined in this experiment is

$$He^+(1s)+e^-\rightarrow He^{**}(nln'l')\rightarrow He^*(1sn'l')+h\nu\ , \qquad (1)$$

with $n'\geq n$ and $n=2$. This relatively simple system has been investigated several times with successively better results [11,12,13]. In this paper we report a He^+ DR experiment using a cooled ion beam. Use of cold beams improves the energy resolution by reducing the thermal spread in ion velocities and thereby reducing the spatial overlap of the interacting beams. High resolution is important for this measurement because, though the spectrum of doubly excited states is relatively simple for a two-electron system, the energy spacings in helium are the smallest overall for any heliumlike system [14,15]. Additionally, theoretical calculations involving helium are influenced by electron correlation, since this contribution to the electrons' orbitals is largest for this lowest-Z two-electron system [16]. High-resolution studies of dielectronic recombination provide a test of these calculations.

Three important processes take place in a cooler storage ring as the ions pass through the electron bath, with relative strengths determined by the center-of-mass-energy. (1) Ion beam cooling: At zero relative energy the ions are thermally coupled to the cold electrons through Coulomb collisions. The ion beam is thereby cooled to an equilibrium temperature somewhat higher than, but related to, the electron temperature, which is typically 1200 K. This effect is further enhanced by an apparent longitudinal cooling due to the transformation to the ion's center-of-mass frame. The latter effect is kinematic rather than thermodynamic, and the resulting spread in ion energies is also further reduced in the longitudinal direction. (2) Radiative recombination: This process takes place at all relative energies, but has a strong maximum at zero relative energy. This can be understood qualitatively by noting that at zero kinetic energy the electron is bound to the ion, regardless of their relative distance of separation, due to the infinite range of the Coulomb interaction. Thus the cross section for electron capture is expected to be infinite. However, the recombination *rate* is finite in practice. This is due to the infinite duration of the capture process at zero relative velocity. Also, because the free electrons have a distribution of velocities,

*Formerly the Manne Siegbahn Institute of Physics.

only an infinitesimal number have zero relative velocity. (3) Dielectronic recombination: At specific energies, dielectronic capture resonances are excited. Those doubly excited systems which stabilize through photon emission retain the captured electron. This capture process is resonant in the free-electron energy because, as the electron is captured, its kinetic energy, as well as any binding energy liberated by the capture, is transferred to a bound electron, which must make a discrete transition.

II. EXPERIMENT

CRYRING is a heavy ion synchrotron-storage ring [17]. The ions are injected into the ring at 300 keV/u from a radio frequency quadrupole (RFQ) accelerator, which is in turn injected from a plasmatron ion source, MINIS. They are then accelerated, as they circulate in the ring, to the fixed velocity of the electron beam. The main advantages of beams merged in this way are the following: (1) In the center-of-mass frame the ions are immersed in a bath of cold electrons. Cold here means a thermal distribution of approximately $kT \sim 0.1$ eV. The radial cross section of the ion beam, which is related to the beam temperature, contracts to a minimum within roughly 1 s [18]. This sharpens the electron-ion interaction energy. (2) The transformation of electron energy fluctuations, as from power supply noise, for example, to the center-of-mass frame greatly reduces their magnitude. In this way the longitudinal component of the electron-beam energy distribution is reduced by several orders of magnitude. Together, these features provide a rather substantial improvement in energy resolution over experiments employing fixed targets.

At CRYRING, ions for which $q/A \geq 0.25$ can be injected and stored at energies up to $96(q/A)^2$ MeV/u. The ring itself is $L = 51.63$ m in circumference, and the ions are confined radially by 12 equally spaced 30° dipole magnets. The ring is equipped with an electron cooler which, by merging a velocity-matched electron beam tangentially with the circulating ions, reduces the internal energy spread of the ions. Experimentally, the single-electron He^+ system has the advantage of producing a neutral recombination product. Thus separation of the recombined ions from the primary beam is easily accomplished by the first dipole magnet following the cooler. The neutrals are detected by a surface-barrier detector (SBD), which is mounted on the cooler axis beyond the first post-cooler dipole magnet. This detector has an efficiency of $\sim 100\%$, and each detected recombination is recorded according to the electron energy at that instant. The SBD can be withdrawn from the beam path to allow the neutrals to strike a 40-mm position-sensitive channel plate detector, also located on the cooler axis. While the efficiency of this detector is only $\sim 50\%$, this setup provides a means of monitoring the radial ion density and gives a qualitative indication of the transverse temperature of the circulating beam.

In CRYRING the electron-beam radius is $r_b = 2$ cm, and the electron current used in this experiment was $I = 0.261$ A. This gives an electron density of $n_e = 2.9 \times 10^7$ cm^{-3} at the cooling energy. He^+ ions circulated in the ring at 869.765 kHz, as determined by a Schottky noise detector. This number is believed to be the most accurate quantity measured in this experiment, and calibration of the beam energy, as well as an estimation of the total number of circulating ions, is made using it. Since the circumference of the ring is 51.63 m, this frequency corresponds to an ion velocity of $v_i = 4.5 \times 10^7$ m/s or 0.1497 c. Their energy is thus 10.7 MeV/amu, and that of the velocity matched cooling electrons is 5.823 keV. Though the electron and ion beams are merged along a physical distance of approximately 1 m, the electron cooler has an effective length, in this experiment, of approximately 0.72 m, as described below. The ions thus spend approximately 1.4% of their time immersed in the electron beam.

The decay of the circulating beam is exponential, with an estimated lifetime of 7.95 s. This estimate was obtained by observing the decay of the ion beam's magnetic field using a beam current transformer. The storage time of these ions is most strongly affected by stripping of the 1-s electron through collisions with residual gases in the ring. During this experiment the average ring vacuum was 2×10^{-11} torr. Table I displays several important experimental parameters.

Data for DR were obtained by scanning the electron energy continuously between center-of-mass energies of 25 and 55 eV. Each data set contains two scans, one with electron energies higher than the cooling energy and another with electron energies lower than the cooling energy. The scans, which follow a 2- or 4-s cooling interval, yield events distributed over 1200 energy channels in a period of 900 ms. Thus data are collected for 0.75 ms at each channel. Data collection was repeated in this way for 740 cycles in each of two complete data sets. The only parameter which was changed between the two data sets was the cooling interval, which was 2 s for one set, and 4 s in the other. No significant difference was observed, we therefore concluded that the beam was essentially cooled within 2 s. Further evidence of beam cooling was obtained by observing the neutral ions on a position-sensitive channel plate detector in line with the cooler axis. The radial beam profile obtained in this way is shown in Fig. 1.

TABLE I. Values of several important experimental parameters.

Parameter		Value
Ion energy	ϵ_i	10.7 MeV/u
Cooling energy	ϵ_c	5.823 keV
Transverse temperature	$kT_\perp$	0.15 eV
Longitudinal temperature	$kT_\parallel$	0.8×10^{-4} eV
Electron-beam radius	r_b	2.0 cm
Electron-beam density	n_e	2.9×10^7 cm^{-3}
Ion-beam radius	r_i	0.9 mm
Number of stored ions	N_i	1.2×10^8
Ring circumference	L	51.63 m
Interaction length	l	0.72 m
Ring pressure	P	2×10^{-11} Torr
Beam lifetime	τ	7.95 s

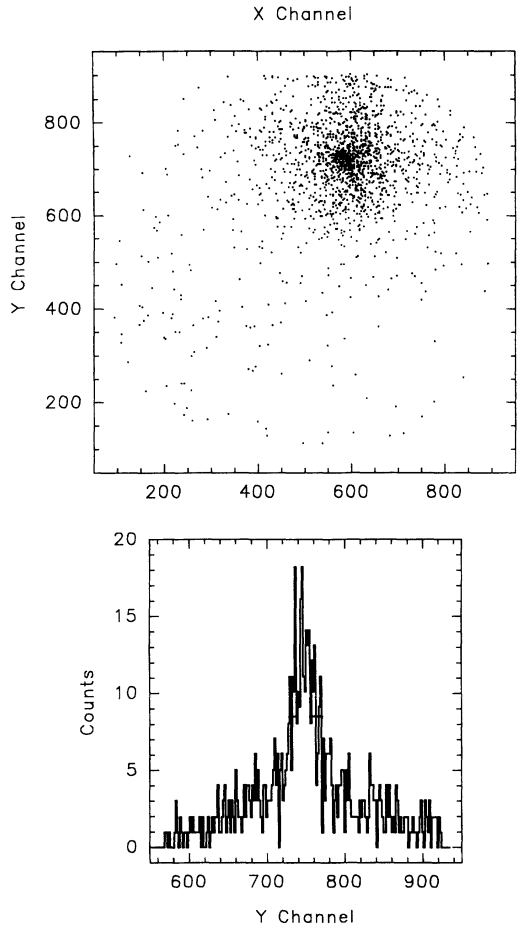

FIG. 1. Top: Radial profile of the ion beam. The intense spot is formed as neutral ions strike a position-sensitive detector directly beyond the electron cooler. The neutral ions pass undeflected through the first post-cooler dipole magnet, therefore retaining the ion beam's radial density profile. Bottom: Projection of the beam profile onto the y axis. From this it is found that the beam has a diameter of 1.8-mm FWHM.

The measured ion-beam diameter was less than 2-mm full width at half maximum (FWHM), which indicates a well-cooled beam. It is interesting to note that the interaction rate does not depend directly on this diameter, since the narrower beam is completely surrounded by electrons in the cooler; the resulting overlap area covers only $\sim 0.25\%$ of the electron beam. The width of the ion beam is determined by the spread in transverse ion energies, i.e., the ion-beam temperature. Since the electron energy varies with distance from the axis, as described below, ions far from the axis would encounter different interaction energies. The manifestation of this would be a distortion of the expected resonance line shape; no such distortion was observed.

III. RESULTS AND DISCUSSION

A. Analysis of resonance line energies

Measurement of the dielectronic recombination resonance energies requires the estimation of several experimental parameters which are not made with spectroscopic accuracy. Further, resonance energies are defined in the center-of-mass frame, requiring the transformation of experimental values. The nonrelativistic transformation to the center-of-mass energy ϵ_0 is

$$\epsilon_0=(\sqrt{\epsilon_c}-\sqrt{\epsilon_l})^2 \tag{2}$$

where ϵ_c is the cooling energy, and ϵ_l is the electron energy in the laboratory frame (the relativistic analog of this equation was used in the data analysis). The value of ϵ_c is limited by the combined accuracy in measurements of the Schottky frequency and the circumference of the ring. The value of ϵ_l, however, is known only to the accuracy of several experimental parameters. These include the values of the electron-beam diameter, the beam tube diameter, the electron-beam current, the amount of space-charge neutralization (which may vary with the electron energy as the resonances are scanned), the relative position of the electron and ion beams, and the deconvolution of the experimental resonance peaks. However, the most important quantity involved is the calibration of the cathode potential. This value may have an error of a few volts, and may have, in addition, small fluctuations due to noise. A precision high-voltage probe was employed for calibration of the cathode voltage during the experiment. Fluctuations in the output voltage, however, were larger than those expected of the cathode high-voltage supply. We therefore binned the experimental data into channels according to a digital signal generated by the ring's master control computer. Use of this signal eliminates peak-broadening effects due solely to noise pickup by the probe, leaving only broadenings due to true variations in the cathode voltage. The correspondence between the digital signal and a linear fit to the probe output is used in the energy analysis. Use of this signal, however, does not eliminate errors in absolute calibration.

An accurate determination of the total space charge must take into account the contribution of positive ions which are trapped in the interaction region by the electron beam's space charge. These ions, produced through ionization of background gases by the high-energy electrons, tend to cancel some portion of the electron beam's space charge. To estimate this space-charge neutralization, represented by the parameter $\zeta < 1$, we first obtain an accurate value of the electron velocity from the Schottky frequency. This determination relies on the fact that, through the collisional drag force between the electron and ion beams, their average velocities are exactly matched. The energy of the electrons in the cooler is related to the cathode potential by

$$\epsilon_e = eV_{\text{cath}} - \left[\frac{1}{v_e}-\frac{\zeta}{v_c}\right]\frac{Ir_c m_e c^2}{e} \times\left[1+2\ln\left[\frac{r_t}{r_b}\right]-\left[\frac{r}{r_b}\right]^2\right], \tag{3}$$

where I is the electron current, r_c is the classical electron radius, v_c is the velocity of the electrons at the cooling energy as determined by the Schottky frequency, v_e is the electron velocity, r_t and r_b are the radii of the beam tube

and the electron beam, respectively, and r is the distance from the electron-beam axis. To a first approximation the ion beam is aligned with the electron-beam axis, since the Schottky signal used to tune the beam has a minimum peak width when the ion beam is on axis, and the space charge varies quadratically from the axis (thus an ion beam tilted with respect to the electron-beam axis will produce a broader Schottky peak which increases with the angular error). In this experiment, we found a neutralization $\zeta=0.12$, so that $\approx 12\%$ of the electron-beam space charge was neutralized. This value was obtained by setting $v_e=v_c$ in Eq. (3) and using the measured value of the cathode voltage. The estimate of ζ is also influenced by errors, if any, in the calibration of the cathode power supply voltage. For example, if this supply is in error by 1 V (out of 5823 V) the value of ζ will automatically compensate. This occurs because we cannot distinguish between voltage differences arising from space-charge neutralization and those from errors in V_{cath}. Note that the neutralization is constant in Eq. (3). In previous studies [12] the neutralization was allowed to vary with the space charge of the electrons or, equivalently, with the electron velocity, by expressing the neutralization as $(1-\zeta)/v_e$. However, by modeling the time evolution of the trapped ion population, we determined that the time constant for such variations is approximately 7 s under our experimental conditions. Since our energy scans take place in less than 1 s, no variation in the neutralization parameter is included.

Once the space-charge neutralization parameter has been found, a transformation from time channel to lab energy is made for each data point. This transformation first requires two linear mappings to obtain an estimate of V_{cath} from the time channel. In principle, one would then insert V_{cath} into Eq. (3) and solve for ϵ. However, v_e is related to ϵ by the relativistic expression $\epsilon=(\gamma-1)m_e c^2$, which makes the evaluation of ϵ nontrivial. We therefore estimate v_e nonrelativistically using eV_{cath} to obtain an intermediate value of ϵ. This energy must be used, in turn, to find v_e so that a more accurate electron energy can be calculated. This iterative process converges very rapidly, so that Eq. (3) is evaluated only three times. This calculation is repeated for each energy value in the data sets.

The energy position of the $2s2p\,^3P$, at 33.724 eV [19], and our calculated average position of the $2l5l'$ group of resonances were used as benchmarks in the estimation of the experimental line positions, though a larger uncertainty arises for the higher-energy point. Although our calculated energy positions (see Sec. III B) for the lower-energy resonances are unreliable for energy calibration, examination of the positions of the higher resonances shows that as the series limit is approached they agree closely with a modified Rydberg formula of the form $\epsilon_d=\epsilon_I-\xi/n^2$, where ϵ_d is the energy of the doubly excited state, ϵ_I is the energy of the series limit at 40.818 eV, and ξ is a screening parameter approximately equal to 16 eV. We also note that some uncertainty in the position of this spectral feature may arise from the necessary reliance on the estimated resonance strengths it contains. The overall energy uncertainty is estimated to be 0.05 eV. When compared to these values, our experimental energies were low by roughly 0.2 and 0.4 eV for the high $\epsilon>\epsilon_c$ and low $\epsilon<\epsilon_c$ energy scans, respectively. Since the high- and low-energy scans do not yield the same line positions, we believe that the discrepancy results from a small error in the linear transformation parameters. Insight into the magnitude of the errors involved can be found by observing that an error of 2 V in the reading of the relative change in cathode voltage as the resonances are scanned could give this shift in line positions. It is interesting to note that the experimental energies are shifted by $\sim 1\%$, which is only half the size of the difference between relativistic and classical calculations of these energies.

In order to compare our data to convoluted theoretical cross sections, it is important that the experimental resonance peaks have the correct line positions. Therefore, both high- and low-energy data sets were adjusted to coincide with the benchmark positions described above using linear transformations. The effect of these shifts on the shape of the resonance peaks, while small, is expected to make them conform more closely to the actual center-of-mass profile. Transformed experimental data are shown in Fig. 2.

The experimental energy resolution can roughly be estimated from Fig. 3, which displays the experimental result for the $\epsilon>\epsilon_c$ scans. The peak width is seen to be ~ 0.3-eV FWHM. The peaks also exhibit the asymmetric line shape typical of flattened thermal energy distributions. We therefore fit the four $2l2l'$ peaks with standard functions used for peak analysis in such cases [20]. These flattened thermal distributions are Gaussians in velocity space, but are asymmetric in energy, with a

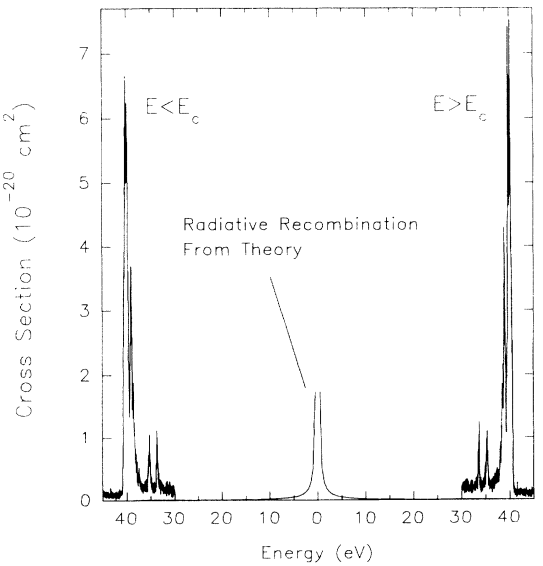

FIG. 2. Transformed experimental results. The data on the left were obtained with electron velocities lower than that of the ions, and the data on the right with larger electron velocities. The smooth curve is the calculated radiative recombination cross section, shown for comparison.

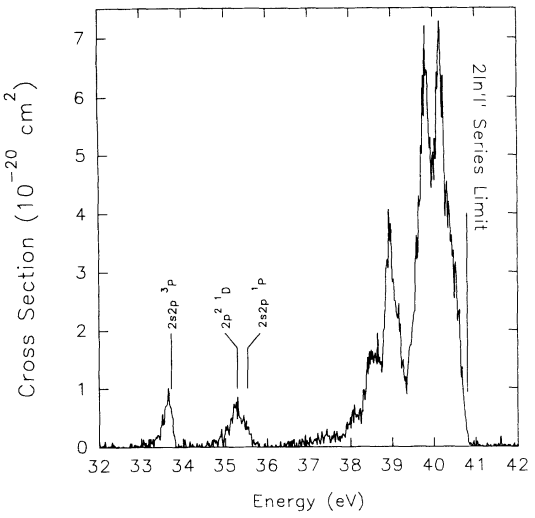

FIG. 3. He^+ dielectronic recombination cross sections. This result is an average of two spectra taken for electron energies greater than the cooling energy. The line positions have been shifted by approximately 0.2 eV to coincide with spectroscopic values, and the background has been subtracted.

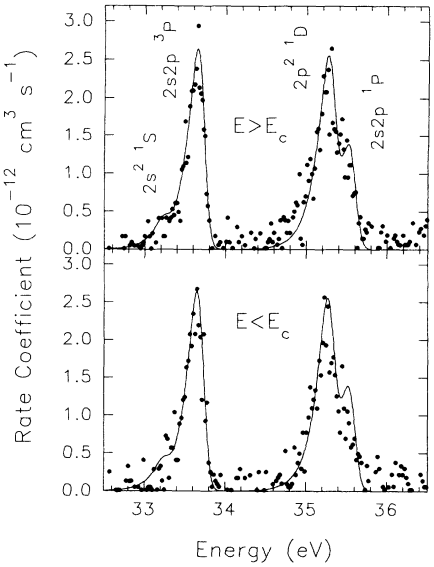

FIG. 4. Fits to the $2s^2\,{}^1S$, $2s2p\,{}^3P$, $2p^2\,{}^1D$, and $2s2p\,{}^1P$ peaks. From these fits the transverse and longitudinal ion temperatures, shown in Table I, were estimated, and the experimental cross sections evaluated. Due to statistical uncertainties, the intensity of the $2s^2\,{}^1S$ resonance is given an upper bound of 0.02×10^{-20} cm^2 eV.

peak in density near zero and an infinite tail extending to higher energies. This can be understood by noting that the transverse distribution dominates the line shape, and that it only adds to the externally set interaction energy. As the electron energy is scanned, a sharp resonance appears roughly as a mirror image of the energy density curve.

Before the fits were made, the entire spectrum was adjusted to ensure that the peak positions coincided with the best available spectroscopic values. Parameter values obtained from fits to the $2l2l'$ states are included in Table I. The best-fit values for the transverse and longitudinal temperatures are $kT_\perp \approx 0.15$ eV and $kT_\parallel \approx 0.8\times10^{-4}$ eV, respectively. However, the $2s2p\,{}^3P$ resonance has a natural linewidth of approximately 0.007 eV [21], which, together with a fit to only one isolated resonance, contributes to the error bars for these parameters. The results of the fits are shown in Fig. 4.

The expected values for the transverse and longitudinal temperature parameters are given by [22]

$$T_\perp = T_{\rm cath}$$
$$T_\parallel = \frac{kT_{\rm cath}^2}{4\epsilon_c} + \left[\frac{2m_e c^2 r_e}{k}\right]\left[\frac{4\pi n_e}{3}\right]^{1/3}, \tag{4}$$

where $T_{\rm cath} = 1173$ K (0.1 eV) is the cathode temperature, ϵ_c is the electron cooling energy, r_e is the classical electron radius, and n_e is the electron density. $T_\perp = T_{\rm cath}$ since no transformations take place in the transverse plane, and the electrons are assumed to be fixed in their relative transverse positions by the cooler's solenoidal magnetic field. The first term in the expression for the longitudinal temperature results from the transformation of the electron's thermal energy to a frame of reference traveling at the cooling velocity. This term can be obtained by assigning $\epsilon_l = \epsilon_c + kT_{\rm cath}$ in Eq. (2) and keeping only the first remaining term in a binomial expansion. For our conditions the transformed thermal distribution has an expected temperature $kT_{\parallel\rm therm} = 4.3\times10^{-7}$ eV. The second term arises from the potential energy stored in the electron beam's charge density (cd). After acceleration, the electrons have a distribution of relative separation distances with an average $r_{\rm av} \sim n_e^{-1/3}$. This potential energy is the same in both the lab and moving frames and is added directly to the longitudinal temperature distribution, since the resulting relaxational motion has a random distribution. This effect contributes $kT_{\parallel\rm cd} = 1.4\times10^{-4}$ eV to the longitudinal electron temperature. This energy clearly dominates $kT_\parallel$ and is therefore our expected longitudinal temperature. Differences between these expected temperature parameters and the values obtained by fits to the experimental data may be due to fluctuations in the cathode potential, which contribute to the longitudinal energy spread and transform like the thermal distribution. Beyond the kinematic reduction of the electron-ion interaction temperature in the center-of-mass frame, cooling improves the energy resolution by condensing the ion beam about the electron-beam axis. Subsequent interactions take place within a smaller range of space-charge-shifted electron energies. Misalignment of the electron and ion beams, which contributes to the apparent distribution of electron energies, may account for the higher than expected transverse temperature obtained from the fits. The lower than expected longitudinal temperature may be the result of a slight distortion of the peak shape due to misalignment.

B. Cross sections

Because the ions which undergo recombination are neutral when they exit the cooler, they pass straight through the next dipole magnet and strike the SBD. The rate at which these neutrals are detected is directly related to the corresponding rate coefficient $\alpha(\epsilon)$. The rate coefficient is related to the event rate R by

$$\alpha(\epsilon)=R\gamma^2[n_e(\epsilon)N_i l/L]^{-1}\ , \tag{5}$$

where $\gamma^2(\sim 1.02)$ is the relativistic boost parameter, n_e is the electron density, N_i is the total number of He^+ ions in the ring, l is the length of the electron cooler, and L is the circumference of the ring.

The largest uncertainty in the experiment is in the estimate of the total number of He^+ ions in the ring. A current transformer is used to estimate the circulating ion current [23]. However, a 10% uncertainty exists in these estimates. The measured ion current was typically 17 μA, averaged over a data collection interval of approximately 2 h. From this the average number of He^+ ions circulating in the ring at the start of each cycle was estimated to be $N_i=1.22\times10^8\pm10\%$. An uncertainty also exists in the value of the effective length of the electron cooler, l. Electrostatic pickup elements, which are used to locate the electron-beam position, are installed at the ends of the cooler. Because the diameter of these elements is smaller than that of the main beam tube in the cooler, the space-charge-induced potential on the electron-beam axis, relative to the ground, is higher (less negative) in the region of the pickup elements. The electrons thus increase in energy as they enter this region. During normal operation, a constant voltage ($\simeq$24 V for the present experiment) is placed on the pickups to compensate for this effect at the cooling energy. However, no special provision was made to scale this potential during the energy scans. With such scaling the detuning of the electron energy at the pickups could be minimized. Without this compensation, we expect an additional energy broadening of the observed recombination resonances, and increased uncertainty in the effective cooler length. For the present experiment the effective interaction length was estimated to be $l=0.72\pm0.05$ m.

The cross sections are computed from the DR rate coefficient using the relation

$$\sigma(\epsilon)=\alpha(\epsilon)/\frac{|v_e-v_i|}{1+v_e v_i/c^2}\ , \tag{6}$$

where v_e includes relativistic and space-charge effects. The result is shown in Fig. 2. Identification of the features is made through spectroscopic data on the doubly excited states of helium. The first peak corresponds to the $2s2p\,^3P$ doubly excited state, which has a spectroscopic energy position of 33.72 eV. The feature near 35 eV is the sum of the $2p^2\,^1D$ and $2s2p\,^1P$ resonances. Table II displays integrated experimental cross sections for the major spectral features. Before performing the integrals, and in order to compare the results to theory, the background was subtracted from the cross-section spectra. The calculated radiative recombination cross section for these experimental conditions is also shown in Fig. 2. This curve was generated using Kramer's formula [24,25] including screening [26] and the Gaunt factor [27]. The observed background is not the result of radiative recombination under the DR lines, but results mostly from electron capture from residual gases.

TABLE II. Integrated experimental resonance strengths.

Doubly excited state	Total S_{expt} (10^{-20} cm^2 eV)		Total S_{theor} (10^{-20} cm^2 eV)
	Present	Haar *et al.* Ref. [13][b]	
$2s^2\,^1S$	<0.02		0.0177
$2s2p\,^3P$	0.247±0.031	0.18±0.04	0.254
$2p^2\,^1D$	0.190±0.024		0.185
$2s2p\,^1P$	0.118±0.015	0.21±0.04	0.066
$2l3l'$	2.301±0.262		2.048
$2ln'l', n'=4$–9[a]	5.503±0.621	5.9±0.3	4.52

[a]Convolved theory. Experimental value includes data up to the series limit.
[b]Sum; includes states in row above.

The total resonance strength measured is limited to doubly excited states in which the captured n' electron is not field ionized in the dipole magnet after leaving the cooler. In this experiment, singly excited neutral helium atoms will undergo field ionization if the captured electron occupies a shell with a principal quantum number greater than n_{max} as it transits the magnet. For the ion velocity and dipole field strength used in this experiment $n_{max}\approx5.8$ [28,29]. Therefore, it is expected that contributions to the $2ln'l'$ resonances will be greatly reduced for states with $n'\geq6$. However, a close examination of the spectrum displayed in Fig. 3 shows substantial resonance strength up to the $2ln'l'$ series limit. It is expected that some of the singly excited states with $n'\geq6$ may decay radiatively before reaching the dipole magnet. If this secondary radiative decay of the neutral atom leaves the excited electron in a state below n_{max}, it will thereby avoid field ionization. By secondary radiative decay we mean the second photon emission in

$$\mathrm{He}^{**}(2pn'p)^1D\rightarrow\mathrm{He}^{*}(1sn'p)^1P+h\nu$$
$$\rightarrow\mathrm{He}^{*}(1sn''s)^1S+h\nu'\quad(n''\leq n_{max}\leq n')\ . \tag{7}$$

For example, the lifetime of the $1s6p\,^1P$ state is $\approx$13.1 ns, and that of the $1s7p\,^1P$ state is $\approx$20.7 ns [30], while the average travel time from the electron cooler to the entrance of the dipole magnet is $\sim$41 ns. We therefore expect to observe approximately 96% of the neutral ions produced by recombination into the $2p6p\,^1D$ resonance, and 83% of those produced at the $2p7p\,^1D$ resonance. The $2p8p\,^1D$ and $2p9p\,^1D$ resonances, with lifetimes of 30.8 and 43.7 ns, are expected to yield 74% and 61%, respectively. Estimated contributions from $2pn'p\,^1S$ resonances are roughly 20% of those of the ^1D states. Resonances with $n'\geq6$ have energies close to the series limit at 40.8 eV. Thus the shape of the observed envelope of resonances near the series limit is largely determined by the combined effects of field ionization and the radiative

lifetimes of the highly excited states. While it is important to note that the field-ionization formula is only an estimate, it is believed that the uncertainty in the value of n_{max} is roughly 0.5, so that the presence of states with $n'=7$, 8, or 9 may imply that secondary decay of these states is involved.

Theoretical dielectronic recombination cross sections have been calculated for the $2ln'l'$ resonances, encompassing $l=0$, and 1, and $2\leq n'\leq 9$, with $0\leq l'\leq 6$. The isolated resonance approximation (IRA) was used together with an accompanying *LS*-coupling scheme [31]. We have found that intermediate coupling and configuration mixing effects within the $2n$ manifold are negligible. Except for the *KLL* resonances, the $1s$, $2s$, and $2p$ orbitals were taken to be hydrogenic. However, our Rydberg and continuum configurations were based on a Hartree potential generated from an $n=2$ Slater-type orbital (STO). A Hartree potential was also used to construct the $2s$ and $2p$ orbitals for the *KLL* resonances. The neglect of exchange in the Hartree equation is not a major omission when using STO's. Such a model was repeatedly shown in the past to be very reliable, since it compares favorably with detailed computations which include the local Hartree-Slater exchange effects and more elaborate wave functions. Clearly, the limitations of this relatively simple atomic structure for doubly excited states of helium will lead to errors in the positions of the resonances, as well as to uncertainties in the *KLL* radiative and *KLn'* autoionization rates of typically 20% and 40%, respectively. These estimates are assessed from calculations employing an alternative atomic structure. It has previously been demonstrated that the DR cross sections are more sensitive to errors in the radiative than in the autoionization rates. The total resonance width presently obtained using the IRA contains the approximate radiative *width*. Omission of this width would cause an overestimate by at least a factor of two of the DR cross sections for $n'>2$. The radiative width is not included in the standard implementation of the close-coupling method for photoionization. Such a computation (e.g., of the *R*-matrix type) would otherwise potentially lead to more accurate DR (plus RR) cross sections. Photoionization, as an inverse process, is related to the DR and RR phenomena through the principle of detailed balance. Electron correlation effects must be thoroughly taken into account in obtaining highly accurate doubly excited states of helium. However, this requires a major computational effort [16]. In the present calculations, which include energies, autoionization, and radiative rates for hundreds of levels, electron correlation is included only through the use of antisymmetrized wave functions and limited configuration interaction (CI) [25].

Theoretical cross sections have been convoluted with the energy distribution function using electron temperatures obtained from the experimental data. The resulting envelope of convolved cross sections is displayed in Fig. 5 along with the experimental data up to the $n=2$ series limit. Besides the comparison of integrated cross sections shown in Table II, several interesting features appear. As noted above, the theoretical peak positions are shifted somewhat from their spectroscopic values, especially for

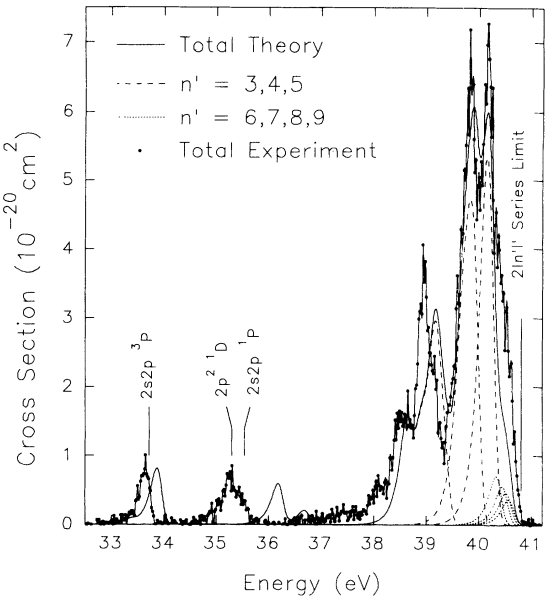

FIG. 5. Comparison of the experimental results with convolved theoretical cross sections. The $n'=2$, 3, 4, and 5 resonances are shown separately. The $n'=6$, 7, 8, and 9 curves include only the $2pn'p\,^1D$ resonances, some fraction of which are expected to avoid field ionization through secondary photo decay prior to reaching the post-cooler dipole magnet. The resulting total theoretical cross section is shown by the smooth curve. See the text for comments on the line positions.

the $2l2l'$ and $2l3l'$ doubly excited states. Also, the experimental peaks are expected to be approximately 0.07 eV lower than the actual resonance positions due to the asymmetric nature of the experimental line shape. Plots of the convolved theoretical cross sections for resonances within the separate orbital shells $n'=3$, 4, and 5 reveal that the first of the two large peaks is largely made up of $n'=4$ resonances, and that the second large peak contains mostly $n'=5$ resonances. However, the experimental data clearly contain contributions from states with $n'\geq 6$. Convolved theoretical cross sections for the surviving fraction of $n'=6$, 7, 8, and 9 resonances (see discussion above) are shown separately for comparison. The figure indicates that the theoretical cross sections are slightly lower than the measured intensities of the $n'=4$ and 5 resonances, and that there may be additional contributions by resonances beyond the estimated n_{max} cutoff.

The uncertainty in the measured cross sections includes three main contributions. The beam current transformer [23] used to estimate the ion current has an estimated uncertainty of approximately 10%, and as shown by Eq. (5) the measured cross sections depend directly on this quantity. The interaction length within the electron cooler has an estimated uncertainty of 7%. Finally, we include a rough estimate of the statistical uncertainty, which is typically 5%. The uncertainties reported in Table II reflect those combined contributions.

IV. CONCLUSION

We have measured the dielectronic recombination cross sections of stored and cooled hydrogenlike helium in a cooler storage ring. An experimental energy resolution of 0.3-eV FWHM was achieved. Fits to the $2l2l'$ resonances were made, and the values $kT_{\perp} \approx 0.15$ eV and $kT_{\parallel} \approx 0.8 \times 10^{-4}$ eV were found for the electron temperature distribution. Integrated resonance strengths are reported for the $2ln'l'$ series of resonances. The results are in qualitative agreement with resonance strengths calculated using a Hartree potential with Slater-type orbitals. The observed cross sections include contributions from capture into states above the estimated field-ionization limit, providing evidence of secondary radiative decay of high n states in the singly excited neutral atom.

ACKNOWLEDGMENTS

The authors would like to thank the staff and technicians of CRYRING for their assistance in this experiment. The authors also thank Dr. Dž. Belkić for helpful discussions. This work was supported by the Swedish Natural Science Research Council and the Knut and Alice Wallenberg Foundation. One of the authors (M.P.) acknowledges the partial support provided by the KBN, Grant No. 2P30205604.

[1] A. Burgess, Astrophys. J **139**, 776 (1964).
[2] H. S. Massey and D. R. Bates, Rep. Prog. Phys. **9**, 62 (1942).
[3] M. J. Seaton and P. J. Storey, in *Atomic Processes and Applications,* edited by P. G. Burke and B. L. Moisewitsch (North-Holland, Amsterdam, 1976).
[4] J. Dubau and S. Volonte, Rep. Prog. Phys. **43**, 199 (1980).
[5] D. A. Knapp, R. E. Marrs, M. A. Levine, C. L. Bennett, M. H. Chen, J. R. Henderson, M. B. Schneider, and J. H. Scofield, Phys. Rev. Lett. **62**, 2104 (1989).
[6] P. Beiersdorfer, T. W. Phiilips, K. L. Wong, R. E. Marrs, and D. A. Vogel, Phys. Rev. A **46**, 3812 (1992).
[7] R. Ali, C. P. Bhalla, C. L. Cocke, and M. Stockli, Phys. Rev. Lett. **64**, 633 (1990); Phys. Rev. A **44**, 223 (1991).
[8] D. R. DeWitt, D. Schneider, M. H. Chen, M. B. Schneider, D. Church, G. Weinberg, and M. Sakurai, Phys. Rev. A **47**, R1597 (1993).
[9] W. Spies, A. Müller, J. Linkemann, A. Frank, M. Wagner, C. Kozhuharov, B. Franzke, K. Beckert, F. Bosch, H. Eickhoff, M. Jung, O. Klepper, W. König, P. H. Mokler, R. Moshammer, F. Nolden, U. Schaaf, P. Spädtke, M. Steck, P. Zimmerer, N. Grün, W. Scheid, M. S. Pindzola, and N. R. Badnell, Phys. Rev. Lett. **69**, 2768 (1992).
[10] A. Wolf, J. Berger, M. Bock, D. Habs, B. Hochadel, G. Kilgus, N. Neureither, U. Schramm, D. Schwalm, E. Szmola, A. Müller, M. Wagner, and R. Schuch, Z. Phys. D **21**, 69 (1991).
[11] J. A. Tanis, E. M. Bernstein, S. Chantrenne, M. W. Clark, T. Ellison, C. C. Foster, W. G. Graham, W. W. Jacobs, J. R. Mowat, T. Rinckel, A. Ross, D. Schneider, M. P. Stockli, and N. R. Badnell, Nucl. Instrum. Methods B **56/57**, 337 (1991).
[12] T. Tanabe, M. Tomizawa, K. Chida, T. Watanabe, S. Watanabe, M. Yoshizawa, H. Muto, K. Noda, M. Kanazawa, A. Ando, and A. Noda, Phys. Rev. A **45**, 276 (1992).
[13] R. R. Harr, J. A. Tanis, V. L. Plano, K. E. Zaharakis, W. G. Graham, J. R Mowat, T. Ellison, W. W. Jacobs, and T. Rinckel, Phys. Rev. A **47**, R3472 (1993).
[14] G. Kilgus, J. Berger, P. Blatt, M. Grieser, D. Habs, B. Hochadel, E. Jaeschke, D. Kramer, R. Neumann, G. Neureither, W. Ott, D. Schwalm, M. Steck, R Stokstad, E. Szmola, A. Wolf, R. Schuch, A. Muller, and M. Wagner, Phys. Rev. Lett. **64**, 737 (1990).
[15] D. R. DeWitt, D. Schneider, M. W. Clark, M. H. Chen, and D. Church, Phys. Rev. A **44**, 7185 (1991).
[16] U. Fano, Rep. Prog. Phys. **46**, 97 (1983).
[17] K. Abrahamsson, G. Andler, L. Bagge, E. Beebe, P. Carlé, H. Danared, S. Egnell, K. Ehrnstén, M. Engström, C. J. Herrlander, J. Hilke, J. Jeansson, A. Källberg, S. Leontein, L. Liljeby, A. Nilsson, A. Paal, K.-G. Rensfelt, U. Rosengard, A. Simonsson, A. Soltan, J. Starker, and M. af Ugglas, Nucl. Instrum. Methods B **79**, 269 (1993).
[18] H. Danared, Phys. Scr. **48**, 405 (1993).
[19] Stanley Bashkin and John O. Stoner, Jr., *Atomic Energy Levels and Grotrian Diagrams* (North-Holland, Amsterdam, 1975).
[20] G. Kilgus, D. Habs, D. Schwalm, A. Wolf, N. R. Badnell, and A. Müller, Phys. Rev. A **46**, 5730 (1992).
[21] H. Cederquist, M. Kisielinski, and S. Mannervik, J. Phys. B **16**, L479 (1983).
[22] H. Poth, Phys. Rep. **196**, 135 (1990).
[23] K. B. Unser, CERN Report No. SL/91-42 (BI) (1991) (unpublished).
[24] H. A. Kramers, Philos. Mag. **46**, 836 (1923).
[25] R. D. Cowan, *The Theory of Atomic Structure and Spectra* (University of California Press, Berkeley, CA, 1981).
[26] L. H. Andersen and J. Bolko, J. Phys. B **23**, 3167 (1990).
[27] D. C. Griffin, Phys. Scr. T **28**, 17 (1989).
[28] C. Bottcher, D. C. Griffin, and M. S. Pindzola, Phys. Rev. A **34**, 860 (1986).
[29] A. Müller, D. S. Belic, B. D. DePaola, N. Djuric, G. H. Dunn, D. W. Mueller, and C. Timmer, Phys. Rev. Lett. **56**, 127 (1986).
[30] Constantine E. Theodosiou, At. Data Nucl. Data Tables **36**, 97 (1987).
[31] M. S. Pindzola, N. R. Badnell, and D. C. Griffin, Phys. Rev. A **42**, 282 (1990).